Photocatalytic Degradation of Environmental Pollutants by Solar Light Using Fabricated $BaPbCe_2O_7$ Nanomaterial

Tejveer Singh Tanwer[1], Jinesh Menaria[2], Dushyant Kumar Prajapati[3], Jeevan Kunwar Chouhan[4], Shipra Bhardwaj[5]

[1,2,3,4,5]*Department of Chemistry, Government Meera Girls College, Mohan Lal Sukhadia University, Udaipur, Rajasthan, India*

***Abstract*—A novel nano-photocatalyst $BaPbCe_2O_7$, was successfully synthesized via a controlled co-precipitation method, followed by calcination, yielding 73% of the final product. The structural and morphological characteristics of the synthesized material were thoroughly examined using a range of analytical techniques. UV–Vis spectroscopy confirmed an optical band gap of 2.32 eV. The obtained nanoparticles (NPs) were subsequently employed as an efficient photocatalyst for the degradation of malachite green (MG), brilliant green (BG) and crystal violet (CV) dyes. A detailed kinetic analysis was carried out to determine the optimal degradation conditions. Notably, $BaPbCe_2O_7$ demonstrated excellent photocatalytic performance, achieving degradation efficiencies of approximately 87% (MG), 94% (BG) and 81% (CV) within 25 minutes. Scavenger studies confirmed the involvement of reactive radical species in the degradation process. Furthermore, recyclability tests indicated that the photocatalyst retained nearly consistent activity even after five consecutive cycles. A plausible photocatalytic degradation mechanism has also been proposed.**

***Index Terms*—Photocatalysis, Photodegradation, Coprecipitation, Dye degradation, Water treatment.**

I. INTRODUCTION

Malachite green is a triphenylmethane basic dye, readily soluble in water that possesses antimicrobial properties [1], used to dye silk, cotton, leather, wool and paper and it is also employed as a fungicide and disinfectant in the fish farming industry [2]. Brilliant green is the triarylmethane dyes [3], used to dye materials, particularly silk and wood, and is also present in plastic and rubber industries' effluents. Skin contact, eye contact, and the ingestion of this dye are all dangerous [4]. Crystal violet is a triarylmethane dye [5] used as a histological stain and in Gram's method of classifying bacteria. Crystal violet has antibacterial, antifungal, and anthelmintic (vermicide) properties and was formerly important as a topical antiseptic. The medical use of the dye has been largely superseded by more modern drugs [6].

Photodegradation has emerged as a promising contemporary approach to addressing the water pollution. Extensive research has focused on this technique, which not only facilitates the removal of toxic pollutants but also their transformation into non-toxic by-products mediated by light and a photocatalyst [7, 8]. In recent nanotechnology breakthroughs, metal oxide nanoparticles (NPs) have become crucial for various technological applications, including sensors, photocatalysis, antibacterial treatments, anticancer therapies, energy storage and environmental remediation [9]. Among different metal oxide NPs, TiO_2, SnO_2, ZnO, CuO and BaO have been extensively studied for their potential in environmental and biomedical applications [10,11]. BaO NPs, with distinct characteristics such as a highly reactive surface, a broad bandgap, narrow emission and strong electrical conductivity, find applications in crown glass production, humidity sensors and photocatalysis, in medical and pharmaceutical fields, diagnostic imaging, orthopedic medicines, in-vitro apoptosis and DNA damage studies [12,13,14]. Furthermore, BaO NPs are attractive candidates for efficient photocatalytic applications due to their high surface-to-volume ratio, superior oxygen adsorption capability, wide availability and cost-effectiveness [15]. Lead oxide (PbO) is recognized as an important

industrial material that can be used in batteries, composite electrode, optical sensor, reusable catalyst and glass industry [16, 17]. Lead oxide, particularly in nanoparticle form (PbO NPs), has shown promising photocatalytic activity due to its unique properties, including its bandgap and ability to absorb light. Taking advantage of their inherent photocatalytic capabilities, such nanoparticles can initiate and enhance degradation reactions when exposed to light, thus providing a sustainable and energy-efficient strategy for treating wastewater. CeO_2 is another semiconductor photocatalyst with various applications. However, its band gap is in the wide range of 2.6 to 3.4 eV, depending on the preparation method [18,19]. The main properties that make CeO_2 significant as a photocatalyst and photoelectrode material applied in the degradation of various pollutants result from its high band gap energy, high refractive index, high optical transparency in the visible region, high oxygen storage capacity, and chemical reactivity [20, 21]. Considering the promising features of quaternary photocatalysts and their vital role in advanced oxidation processes (AOPs), here we report the synthesis, detailed characterization and application of a novel quaternary photocatalyst, $BaPbCe_2O_7$ aimed at efficient dye removal from wastewater systems. The synthesized nanoparticles are characterized in the accepted manuscript aspects of crystalline, morphology, purity, compositional analysis and optical properties via various spectroscopic and analytical techniques. The outcomes of fabrication, characterization and its photocatalytic performance evaluation are elaborately addressed and discussed in further sections.

II. EXPERIMENTAL

2.1 Materials and Method

Barium nitrate, lead nitrate and cerous nitrate (sourced from Merck) were used as precursor materials in the synthesis of the photocatalyst, while sodium hydroxide from CDH was employed as the precipitating agent. To adjust the pH of the solutions, hydrochloric acid (CDH) and sodium hydroxide (CDH) were utilized. UV-Vis spectrophotometry (CHINO) was employed for kinetic study to record the optical density of solutions at various time intervals. For irradiation, a 200Watt tungsten lamp (Philips) was used. Scavengers, namely Isopropanol, EDTA, KI and ammonium oxalate were incorporated to trap active species. All chemicals were utilized in their LR grade, with a purity range of approximately 95-99%.

2.2 Instrumentation

The many techniques used to characterize the produced $BaPbCe_2O_7$ photocatalyst are covered in detail here. pH measurements were conducted using a pH meter (Hena imported pen type). UV-Vis spectrophotometry (CHINO) was used to monitor the optical density changes whereas light intensity was measured using a solarimeter (New CHEM Dt 1307). A Panalytical X Pert Pro X-ray diffractometer was used to record the X-ray diffraction (XRD) pattern using Ni-filtered Cu Ka radiation at 10 kV and 80 mA for monochromatized Cu Ka (k = 1.5418 Å) radiation, with a scan range of 10\2h\80. A Nova Nano FE-SEM 450 (FEI) scanning electron microscope was used to perform scanning electron microscopy (SEM) measurements to examine the surface roughness and morphology of the samples. Using energy dispersive X-ray, SEM imaging conditions were analyzed for composition. Physical Electronics is performed by the XPS spectra (Model: PHI 5000 Versa Probe III analysis). Using a Perkin Elmer FT-IR Spectrum 2 spectrophotometer, Fourier transform infrared (FT-IR) spectra of KBr pellets in the 400–4000 cm^{-1} range were captured. Using a UV-VIS NIR spectrophotometer (Perkin Elmer, U.S.A.), UV-VIS diffuse reflectance spectra (DRS) were measured. A high-resolution transmission electron microscope was employed to monitor the observations using the HRTEM Hitachi H-7500. Using the following formula, the degradation percentage of the dye was calculated:

% degradation = $(C_o - C/C_o) \times 100$

Where C_o and C represent the initial concentration and final concentration of the dye at different time intervals, respectively.

III. RESULTS AND DISCUSSION

3.1 Synthesis and Characterization of $BaPbCe_2O_7$ nanoparticles:

A solid co-precipitation method was employed for synthesis of $BaPbCe_2O_7$ using its precursors barium nitrate, lead nitrate, cerous nitrate and controlled conditions were maintained during the process resulting in a yellow-colored material with yield 45.56

g and the yield percentage was 91.8 %. This was then subjected to calcination at 500°C for 2 hours. The color of the prepared solid changed to black with yield of 33.23 g and the yield percentage was 73 %.

The EDS spectrum of $BaPbCe_2O_7$ NPs confirms the synthesis of $BaPbCe_2O_7$ NPs as Ba, Pb, Ce and O were observed with elemental weight percentages of 13.73, 20.72, 26.62 and 11.2 respectively. X ray diffraction analysis (XRD) proved it to be nano crystalline material with average crystal size to of 58.12 nm. X-ray Photoelectron Spectroscopy (XPS) spectrum of the synthesized nanomaterial revealed distinct peaks at 880.6 and 897.3 eV corresponding to Ce (II) 3d 5/2 and Ce (II) 3d 3/2, suggesting cerium ions in oxidation states of +2 and +4. UV–Vis spectroscopy revealed the optical band gap to be 2.32 eV [22].

3.2 Photocatalytic activity of $BaPbCe_2O_7$ nanoparticles:

To carry out the kinetic study, solution of dyes (MG, BG, CV) is taken in a borosilicate beaker, pH is measured and photocatalyst is added. It is then exposed to light and after certain time intervals, optical density (O.D.) is recorded. A straight line is observed in the plot of 1+ log of O.D. versus time, as shown in figure 1 (a), (b) and (c). Various models, including pseudo-first order and pseudo-second order (Type-1, Type-2, Type-3, Type-4, and Type-5), are studied to understand the degradation process. After analyzing the data, it is observed that the pseudo-first-order model best explains the degradation process. The optimized conditions for the breakdown of various dyes are identified and are as follows:

pH 10.0, 0.18 g of photocatalyst, dye concentration 1.2×10^{-4} M and light intensity 1960 $mWcm^{-2}$ for malachite green (MG) dye, for brilliant green (BG) dye are pH 10, 0.16 g of photocatalyst, dye concentration of 1.8×10^{-4} M and light intensity of 1960 $mWcm^{-2}$ and the optimized conditions for the breakdown of crystal violet (CV) dye are pH 11.0, 0.20 g of photocatalyst, dye concentration of 0.6×10^{-5} M, and light intensity of 1960 $mWcm^{-2}$. Careful control of these factors is crucial for the effective removal of dyes. A typical run for these dyes is given in figure 1(a) (b) (c).

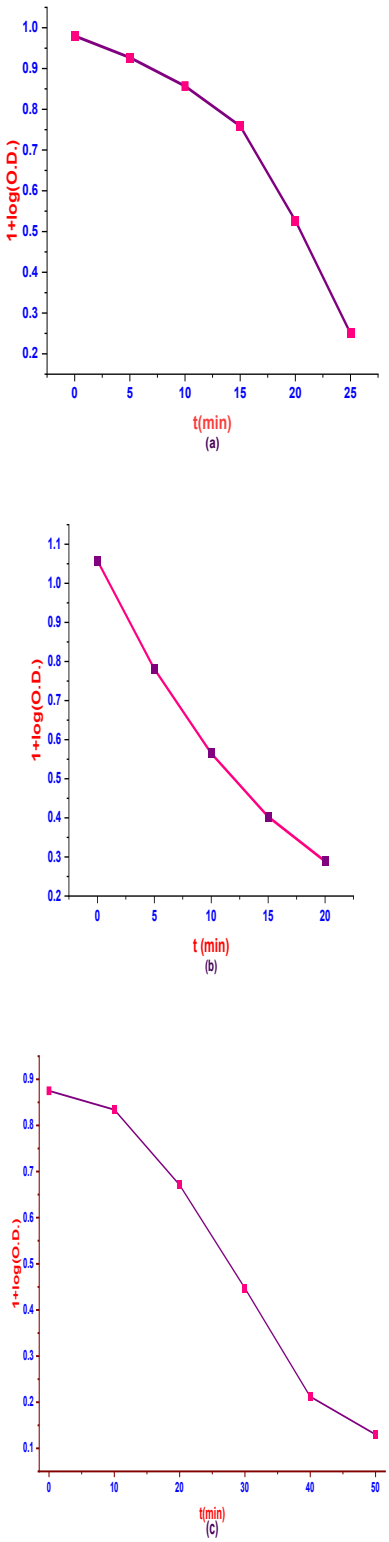

Figure 1: A typical run (a) for MG (b) for BG (c) for CV

3.3 Effect of photocatalyst doses:

The impact of the photocatalyst dosage on the degradation process is meticulously investigated by varying its weight, while ensuring all other variables remain constant. Figure 2 (a), (b) and (c) vividly portray the outcomes of this exploration. Interestingly, the highest degradation rates are observed for MG, BG and CV at photocatalyst dose of 0.18 g, 0.16 g, 0.20 g respectively. The rate constants are presented in table 1. This enhancement can be attributed to the increased surface area available for light absorption, which promotes the generation of a greater number of electron hole pairs thereby enhancing photocatalytic activity. However, upon further increasing the photocatalyst quantity, an interesting trend is observed: the reaction rate begins to decline. This reduction in efficiency is attributed to the enhanced recombination of electron hole pairs at higher catalyst concentrations which suppresses the overall photocatalytic performance.

Table 1: Rate constants at different doses of photocatalyst

Doses of photocatalyst (g/50mL)	MG Rate constant × 10^{-4} (Sec^{-1})	BG Rate constant × 10^{-4} (Sec^{-1})	CV Rate constant × 10^{-5} (Sec^{-1})
0.02	6.417	9.791	-----
0.04	5.190	9.294	-----
0.06	6.582	6.996	3.771
0.08	6.710	6.667	3.383
0.10	6.430	6.615	5.450
0.12	7.158	5.281	4.980
0.14	7.337	5.074	5.090
0.16	7.771	10.107	7.140
0.18	8.444	9.677	7.580
0.20	----	-----	7.950

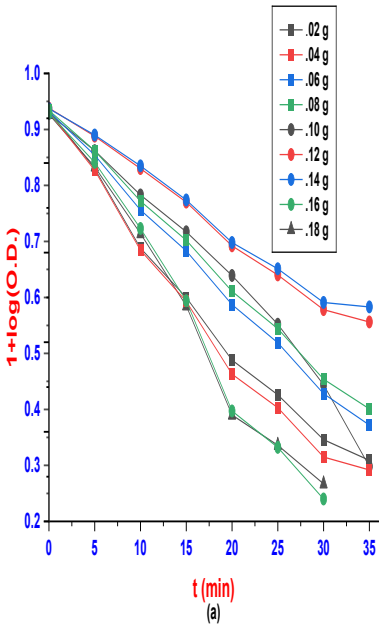

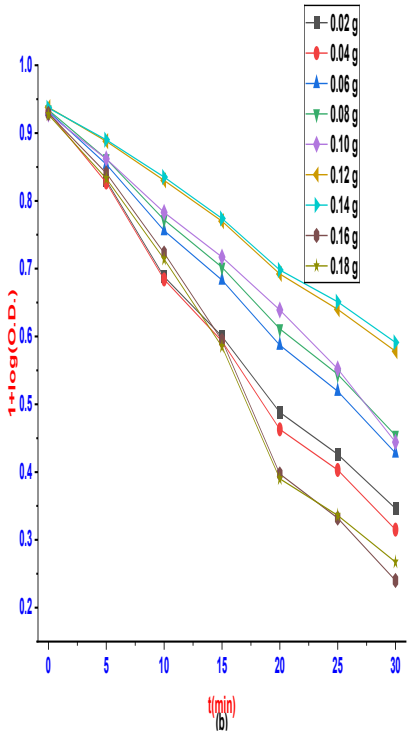

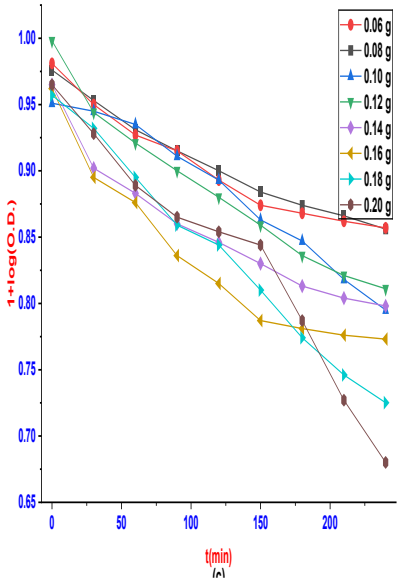

Figure 2. Effect of photocatalyst Dosage (g/50mL)
(a) MG (b) BG (c) CV

3.4 Effect of dye concentration:

The study is conducted within the range of 0.55×10^{-5} to 1.8×10^{-4} M of dye concentration, with all other variables held constant. The resulting data are illustrated in figure 3 (a), (b) and (c) and table 2. Observations indicate that the reaction rate increases with an increase in the concentration of dye. This is because more dye molecules are available to absorb photons from light, becoming excited in the process. However, after reaching a maximum value (at 1.4×10^{-4} M for MG, 1.8×10^{-4} M for BG, 0.6×10^{-5} M for CV), further increase in dye concentration led to a decrease in the rate of degradation. This decline occurs because, beyond a certain concentration, the excess dye intensifies the coloration of the reaction mixture and effectively acts as a filter, reducing the amount of incident light reaching the photocatalyst.

Table 2: Rate constants at different concentrations of dyes

Conc. of Dye x 10^{-4} (moles L^{-1})	MG Rate constant × 10^{-4} (Sec^{-1})	Conc. of Dye x 10^{-4} (moles L^{-1})	BG Rate constant × 10^{-4} (Sec^{-1})	Conc. of Dye x 10^{-5} (moles L^{-1})	CV Rate constant × 10^{-4} (Sec^{-1})
0.2	-----	0.2	7.715	0.55	4.587
0.4	5.761	0.4	7.922	0.60	7.958
0.6	6.052	0.6	6.463	0.65	7.715
0.8	4.968	0.8	7.185	0.70	4.646
1.0	7.418	1.0	5.770	0.75	4.445
1.2	6.384	1.2	5.824	0.80	5.017
1.4	8.444	1.4	6.382	0.85	5.781
1.6	6.578	1.6	6.726	0.90	5.152
1.8	5.026	1.8	8.198		

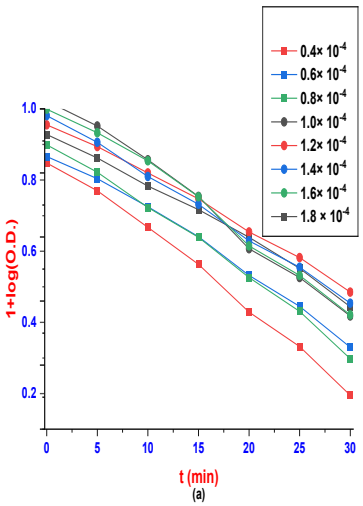

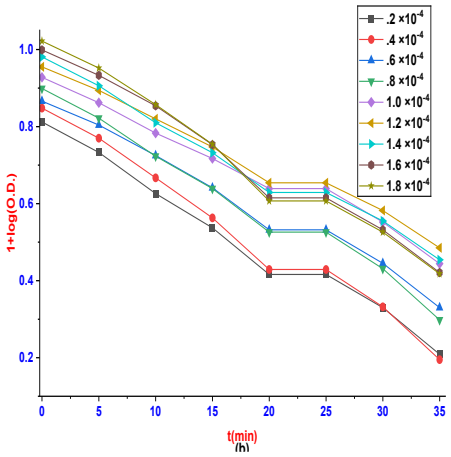

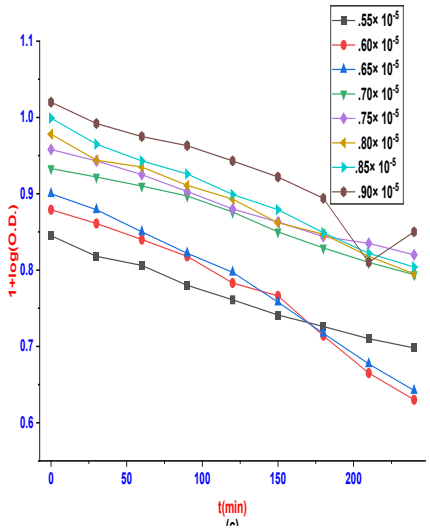

Figure 3. Effect of concentration of dyes (moles L^{-1})
(a) MG (b) BG (c) CV

3.5 Effect of intensity of light:

The experiment entailed adjusting the light intensity within the range of 930 to 1960 $mWcm^{-2}$, with corresponding data presented graphically in figures 4 (a), (b) and (c) and tabulated in table 3. All other experimental variables are kept constant throughout. It is observed that the rate of photocatalytic degradation increased in tandem with the rise in light intensity. This phenomenon can be attributed to the greater number of photons striking per unit area over time as light intensity escalates. Consequently, there is an increase in the presence of excited dye molecules and electron-hole pairs at the photocatalyst's surface. The peak degradation rates are observed at a light intensity of 1960 $mWcm^{-2}$, for all three dyes. Further increase in intensity causes side heat reactions and so are not considered.

Table 3: Rate constants at different intensities of light

Intensity of light ($mWcm^{-2}$)	MG Rate constant × 10^{-4} (Sec^{-1})	BG Rate constant × 10^{-4} (Sec^{-1})	CV Rate constant × 10^{-4} (Sec^{-1})
930	2.861	5.489	4.948
1150	3.024	5.581	5.180
1390	2.938	7.745	5.800
1560	4.663	7.683	6.030
1710	4.543	7.930	7.090
1960	8.444	10.107	7.958

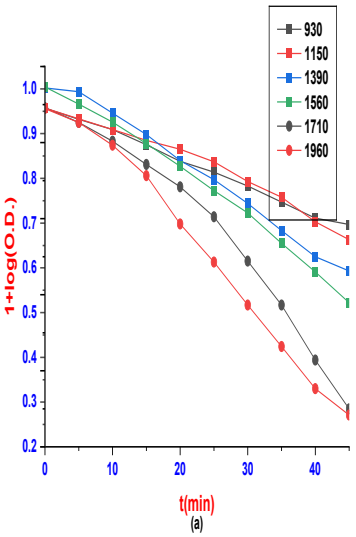

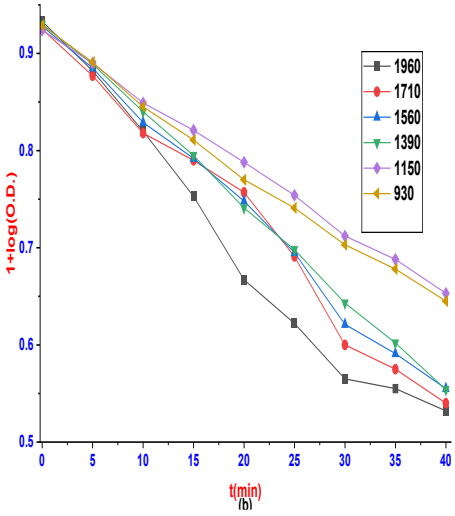

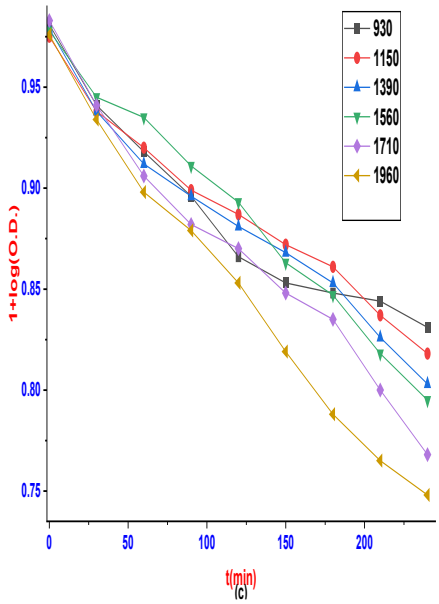

Fig.4. Effect of intensities of light ($mWcm^{-2}$) (a) MG (b) BG (c) CV

3.6 Effect of pH:

The degradation rate of the dye varies markedly with changes in the solution's pH, as many dyes are highly sensitive to pH fluctuations and may even exhibit color shifts under different pH conditions. Thus, pH is considered as the most important factor affecting the degradation of pollutants, especially dyes. To investigate this effect, the pH of the solution was systematically adjusted while maintaining all other parameters constant. Notably, variations in pH resulted in observable changes in the initial optical density of the dye solution, as illustrated in the corresponding graphs. The study focused on the pH range of 6.0 to 10.0 with the results depicted in figures 5 (a), (b) and (c) and rate constants are given in table 4. This thorough analysis reveals how crucial pH is in influencing the dye degradation process. Further increase in pH makes the solution opaque and so is not studied.

Table 4: Rate constants at different pH

pH	MG Rate constant × 10^{-4} (Sec^{-1})	BG Rate constant × 10^{-4} (Sec^{-1})	CV Rate constant × 10^{-4} (Sec^{-1})
6.0	0.291	----	----
6.5	2.168	0.769	0.238
7.0	2.549	4.722	0.601
7.5	4.180	5.628	0.350
8.0	3.596	6.746	0.423
8.5	4.192	7.601	0.496
9.0	5.471	8.650	1.394
9.5	7.176	8.977	6.335
10.0	8.444	10.107	7.958

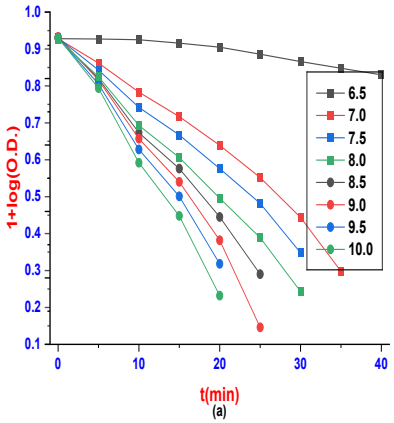

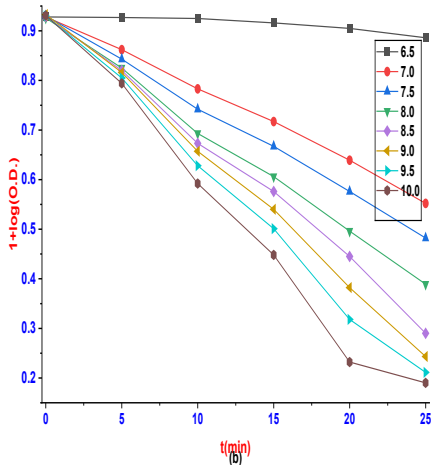

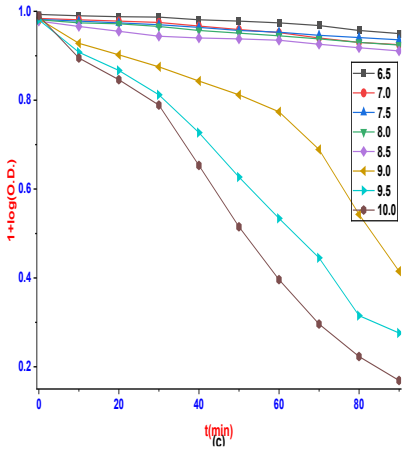

Figure 5. Effect of pH (a) MG (b) BG (c) CV

Various scavengers were employed to determine the specific reactive species involved in the degradation process. The degradation of MG, BG, and CV dyes using the $BaPbCe_2O_7$ nanomaterial was evaluated in the presence of 5 mL of each scavenger EDTA, KI, isopropyl alcohol and anthraquinone. EDTA acted as an effective scavenger for all three dyes (figure 6(a), (b), and (c)) indicating that the •OH radical is the primary reactive species responsible for their degradation. The rate of photocatalytic degradation increases as the pH rises for all three dyes. It is attributed to the fact that increase in pH increases the concentration of OH^- ions and subsequently $OH^\bullet$ free radicals, which are the responsible species for degradation of dyes. Thus, rate of degradation increases. The peak degradation points are observed at pH 10.0. In the presence of the scavenger, the degradation efficiency significantly decreased, stabilizing at only about 5–7% for the dyes, proving the active degradation species to be hydroxyl free radical. [23]

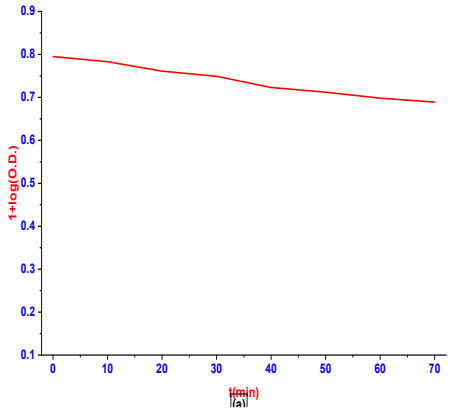

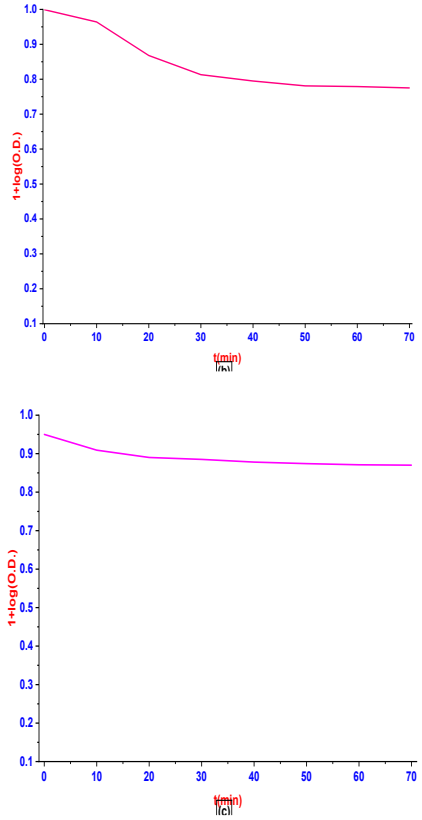

Figure 6. Scavenger study with EDTA (a) MG (b) BG (c) CV

Based on the nature of active species, a tentative mechanism is proposed:

$_1Dye^0 + h\upsilon \rightarrow {}_1Dye^1$ (Excitation of dye molecule from ground state)

$_1Dye^1 + h\upsilon \rightarrow {}_1Dye^3$ (ISC to triplet state)

$BaPbCe_2O_7 + h\upsilon \rightarrow BaPbCe_2O_7 [e^- (CB) + h^+ (VB)]$ (Generation of electron hole pair)

$h^+ + H_2O \rightarrow OH^\bullet + H^+$ (Hydroxyl radical)

MG, BG & CV+ $OH^\bullet \rightarrow NO_2$, CO_2, H_2O etc. (degradation harmless products)

Here Dye molecules in their ground state absorb incident photons and become excited to the singlet state, subsequently undergoing intersystem crossing to the triplet state. Simultaneously, the photocatalyst absorbs photons with sufficient energy to excite electrons from the valence band to the conduction band, generating holes in the valence band. These photogenerated holes facilitate oxidation, while the electrons drive reduction reactions, primarily through the formation of •OH radicals. The highly reactive •OH radicals attack the weaker bonds within the dye molecules, breaking them down into smaller, harmless

end products such as NO_2, CO_2, and H_2O. These benign byproducts minimize environmental harm, underscoring the effectiveness of the photocatalytic degradation process.

3.7 A comparative analysis

A comparative study is carried out for all three dyes and the observations state that BG degrades with faster speed and to a greater extent as compared to MG and CV dyes. The data with maximum conditions are given in table 5.

Table 5: A comparative data analysis for dyes

S. No.	Resulting factors	MG	BG	CV
1	λ_{max} (nm)	620	625	590
2	Conc. of Dye (moles L^{-1})	1.4×10^{-4}	1.8×10^{-4}	0.6×10^{-5}
3	pH	10.0	10.0	10.0
4	Amount of Nanoparticles (g/50 mL)	0.18	0.16	0.20
5	Intensity of Light ($mWcm^{-2}$)	1960	1960	1960
6	Degradation Time (min.)	25	20	50
7	% degradation	87%	94%	81%
8	Rate constant $\times 10^{-4}$ (Sec^{-1})	8.44	10.10	7.95

3.8 Recycling of the photocatalyst

The recovered photocatalyst was washed, recalcined, and reused for subsequent dye degradation cycles. It was observed that its photocatalytic efficiency remained almost unchanged even after five consecutive cycles. This excellent recyclability enhances its potential as a promising photocatalyst for environmental remediation applications.

IV. CONCLUSION

$BaPbCe_2O_7$ nanoparticles were successfully synthesized via the co-precipitation method, yielding 73% after calcination. With an average crystallite size of 58.12 nm, the nanoparticles exhibited excellent photocatalytic efficiency in the degradation of Malachite Green (MG), Brilliant Green (BG), and Crystal Violet (CV) dyes in aqueous media. The photodegradation performance increased with catalyst dosage up to an optimal point. Furthermore, the degradation rate was found to be strongly influenced by the dye concentration, pH, and light intensity. Higher photodegradation efficiencies were achieved at lower dye concentrations, elevated pH levels, and greater light intensities, highlighting the effectiveness and adaptability of the synthesized photocatalyst for environmental remediation applications.

REFERENCES

[1] Oladoye, P. O., Ajiboye, T.O., Omotola, E. O., Oyewola, O. J., Methylene blue dye: Toxicity and potential elimination technology from wastewater. Results in Engineering, 2022, 16, 100678.

[2] Dutta, S., Adhikary, S., Bhattacharya, S., Roy, D., Chatterjee, S., Chakraborty, A., Rajak, P., Contamination of textile dyes in aquatic environment: Adverse impacts on aquatic ecosystem and human health, and its management using bioremediation. J. Environ. Manag., 2024, 353, 120103.

[3] Nandi, K.B., Goswami, A., Purkait, K.M. Adsorption characteristics of brilliant green dye on kaolin. J. Hazar. Mat., 2009, 161, 387-395.

[4] Bhattacharyya, K.G., Sarma, A. Adsorption characteristics of the dye, brilliant green, on neem leaf powder. Dyes Pigment. 2003, 57, 211–222.

[5] Green, Floyd J. The Sigma-Aldrich Handbook of Stains, Dyes, and Indicators. Milwaukee, Wisconsin: Sigma-Aldrich Corp., 1990, ISBN 978-0-941633-22-2, 239–240.

[6] Hodge, H. C., Indra, J., Drobeck, H. P., Duprey, L. P., Tainter, M. L. Acute oral toxicity of methylrosaniline chloride. Toxicol. App. Pharmacol., 1972, 22 (1), 1–5.

[7] Kumar, A., Pandey, G., A review on the factors affecting the photocatalytic degradation of hazardous materials. Mater. Sci. Eng. Int. J., 2017, 1(3), 1-10.

[8] Al-Nuaim, M. A., Alwasiti, A. A., Shnain, Z. Y., The photocatalytic process in the treatment

of polluted water. Chemical Papers, 2023, 77(2), 677-701.

[9] Linic, S., Aslam, U., Boerigter, C., Morabito. M. Photochemical transformations on plasmonic metal nanoparticles. Nat. Mater., 2015, 14, 567-576.

[10] Muthuvel, A., Jothibas, M., Manoharan. C. Synthesis of copper oxide nanoparticles by chemical and biogenic methods: photocatalytic degradation and in vitro antioxidant activity. Nanotechnol. Environ. Eng., 2020, 5,14.

[11] Alarifi, S., Ali, D., Al-Bishri. W. In vitro apoptotic and DNA damaging potential of nanobarium oxide. Int. J. Nanomed., 2016, 11, 249-257.

[12] Renukadevi, R., Sundaram, R., Kaviyarasu. K. Barium Oxide nanoparticles with Robust Catalytic, Photocatalytic and Humidity Sensing Properties. J. Nanostructures., 2020, 10, 167-176.

[13] E. Sundharam, A. Kingson, S. Jeevanraj, C. Chinnusamy. Effect of Ultrasonication on the Synthesis of Barium Oxide Nanoparticles. J. Bionanosci., 2017, 11, 310-314.

[14] Choudhary, R. V., Jha, V., Jana. P. Epoxidation of styrene by TBHP to styrene oxide using barium oxide as a highly active/selective and reusable solid catalyst. Green Chem., 2006, 8 (8), 689-690,

[15] Hamid, A., Khan, M., Hayat, A., Probing the physio-chemical appraisal of green synthesized PbO nanoparticles in PbO-PVC nanocomposite polymer membranes. Spectrochimica Acta Part A: Molecular and Biomolecular Spectroscopy, 2020, 235, 118303.

[16] Sonmez, M.S., Kumar, R.V., Leaching of waste battery paste components. Part 1: Lead citrate synthesis from PbO and PbO_2, Hydrometallurgy, 2009, 95, 53-60.

[17] Sljuki, B., Banks, C.E., Crossley. A., Richard, G., Compton, R.G., Lead (IV) oxide–graphite composite electrodes: Application to sensing of ammonia, nitrite and phenols. Analytica Chimica Acta, 2007, 587, 240–246.

[18] Sharma, D.; Mehta, B.R. Nanostructured TiO_2 thin films sensitized by CeO_2 as an inexpensive photoanode for enhanced photoactivity of water oxidation. J. Alloys Compd. 2018, 749, 329–335.

[19] Prajapati, K.D., Chouhan, K.J., Menaria, J., Tanwer, S.T., Bhardwaj, S. Fabrication and Characterization of Photocatalyst Pb_3CdO_7 for Degradation of Azure- A. J. Environ. Sci. Pollut. Res. 2024, 10, 485–491.

[20] Aboutaleb, W.A., El-Salamony, R.A. Effect of Fe_2O_3-CeO_2 nanocomposite synthesis method on the Congo red dye photodegradation under visible light irradiation. Mater. Chem. Phys. 2019, 236, 121724.

[21] Wang, B., Zhu, B., Yun, S., Zhang, W., Xia, C., Afzal, M., Cai, Y., Liu, Y.; Wang, Y., Wang, H. Fast ionic conduction in semiconductor $CeO_{2-\delta}$ electrolyte fuel cells. NPG Asia Mater. 2019, 11, 51-59.

[22] Tanwer, S.T., Menaria, J., Prajapati, K.D., Chouhan, K.J., Bhardwaj, S. Optoelectronic properties of fabricated $BaPbCe_2O_7$ nanoparticles for photocatalytic breakdown of malachite green: a greener approach. I. J. Creat. Res. Tech., 2025, 13, 2320-2882.

[23] Das, A., Adak, K.M. Kinetic and mechanistic way for photocatalytic degradation of pollutants from textile wastewater by graphene oxide supported nanocomposite. Next Materials Elesvier, 2024, 3, 100.